Pergamon

0734-743X(95)00044-5

Int. J. Impact Engng Vol. 18, No. 4, pp. 369–381, 1996

0734-743X/96 $15.00 + 0.00

MODELLING GEOMETRICAL AND DIMENSIONAL ASPECTS OF BALLISTIC PENETRATION OF THICK METAL TARGETS

R. L. WOODWARD

Counsellor Defence Science, Australian Embassy Washington, 1601 Massachusetts Avenue, NW, Washington, DC 20036-2273, U.S.A.

(*Received* 9 *May* 1995; *in revised form* 8 *August* 1995)

Summary—A simple one-dimensional model is used to examine geometrical and scale effects in the penetration of thick metal targets by projectiles. The model is used in two forms, one assuming the penetrator deforms by mushrooming and the other assuming it is eroded. The mushrooming version gives good predictions of depth of penetration at low velocities where the erosion version overestimates depth of penetration, but at typical ballistic impact velocities the models bound the experimental data from below (mushrooming) and above (erosion). Both versions of the model give good predictions of depth of penetration for low length to diameter (L/D) ratio penetrators at all velocities. The model solutions match experiment in simulating the effect of penetrator L/D ratio and scale and this is attributed to the inclusion of radial inertia and shear effects which are not considered in modified hydrodynamic models of penetration. Differences between penetrator materials based on penetrator strength are also evident in the model computations.

Key words: ballistic impact, penetration mechanics, armour, penetrator L/D ratio, penetrator scaling, finite difference modelling.

NOTATION

d	diameter of a cylindrical element
D	projectile diameter
F	force
h	height of a cylindrical element
L	projectile length
n	constant (material work hardening exponent)
P	depth of penetration
R_t	resistance to penetration (hydrodynamic model)
V	velocity
Y	yield stress
ε	strain
ρ	material density
σ	stress
σ_0	constant (material strength)

1. INTRODUCTION

The modified hydrodynamic theory for the penetration of thick monolithic metal targets by cylindrical projectiles predicts that the depth of penetration (P) divided by the penetrator length (L), or the P/L ratio, is a function of impact velocity and the strengths and densities of the impacting materials, and reaches a maximum at high velocity which depends only on the square root of the relative densities of penetrator and target [1–4]. Maximum depth of penetration at high velocities is achieved by maximizing penetrator length and density. Depth of penetration increases with penetrator length to diameter ratio for penetrators of constant mass. Experimental observations [5–7] have, however, shown that contrary to the simple hydrodynamic theory the relationship between P/L and velocity is not independent of the L/D ratio. Thus Frank and Zook [8] pointed out that small L/D ratio penetrators "*behave like constant mass penetrators*" giving greater effective penetration capability. Efforts have, therefore, focussed on putting both concepts together to obtain maximum penetration performance by making the maximum length penetrator out of many segments, each with

a low L/D ratio. Rosenberg and Dekel [9] have pointed out that the effect of L/D ratio on P/L is easily distinguishable in comparing $L/D = 10$ and $L/D = 20$ performance data. Other parameters which have been shown to differentiate P/L vs velocity data include the scale (or absolute dimensions) of the penetrators and the material type, with tungsten alloy penetrators showing consistently poorer performances than depleted uranium (DU) penetrators of similar strength [10].

One-dimensional models provide useful tools for understanding the physics of penetration processes, for doing parametric studies and for rapid turnaround of performance assessments. There is some advantage, therefore, to be gained in understanding the significance in, and the reasons for, differences between model predictions and experiment. Rosenberg and Dekel [11] approached this by comparing the modified hydrodynamic model with two-dimensional simulations of penetration problems to examine the relationship between the resistance to penetration (R_t) and impact and material parameters. The dependencies of R_t on velocity and target strength observed, suggest some aspects of the physics are not represented in the modified hydrodynamic model. In the present work a one-dimensional model developed by Woodward [12, 13] is used to examine a range of reported experimental data which illustrate the dimension and scale problems with which the modified hydrodynamic approach has difficulty. By taking into account the effects of radial inertia [14, 15] this model has some success in separating out the influences of L/D ratio as observed in experiments. Two concepts are studied where the projectile is modelled as either a mushrooming or an eroding cylinder, these giving better predictions of experimental data at low and high velocities respectively.

DESCRIPTION OF MODELS

The principal features of the Woodward [12, 13] model (referred to as the mushrooming model) are illustrated in Fig. 1(a) in which both the target and penetrator are described

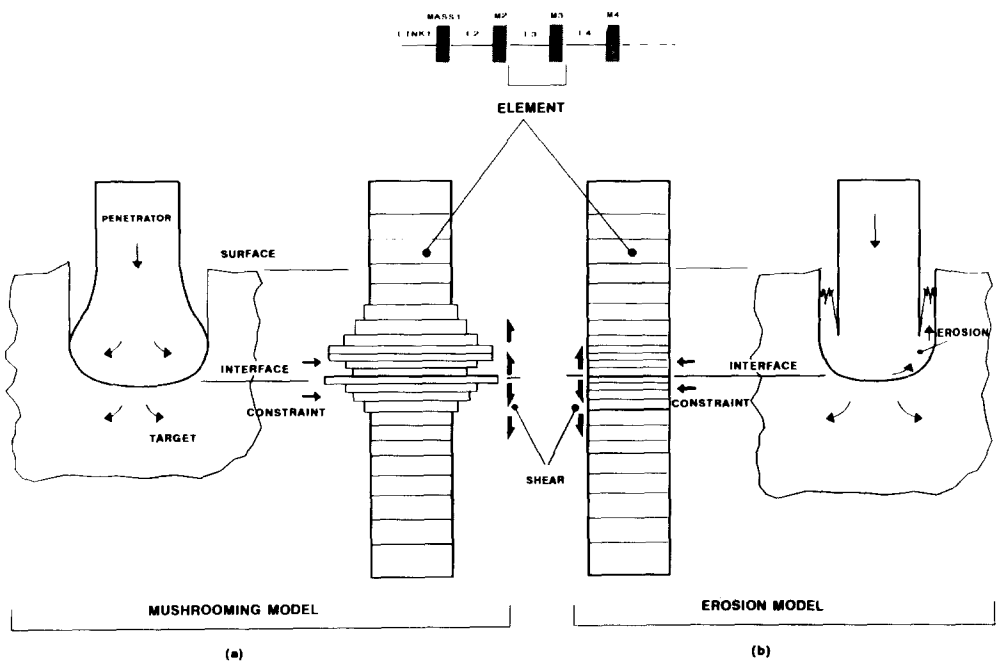

Fig. 1. Concept of the lumped parameter model developed by Woodward [12, 13] showing (a) the original mushrooming version and (b) the erosion version. In the model both the penetrator and target are represented as a stack of cylindrical elements, with each element made up of a link and a point mass. The relationship of the model to the physical problem is indicated schematically for each version.

as cylinders impacting end on, with each cylinder being made of a series of elements characterized by a mass and a ligament, the latter having the stress–strain properties of the material it represents. On impact the cylindrical elements deform in compression. Increased resistance to radial expansion of the element is provided by confinement or constraint where the element diameter either equals or exceeds the hole diameter (defined as the diameter of the interface projectile element) and where the element would also be inside the target (as defined from the original position of the first target element). Resistance is also provided by shear between the element and the target hole wall. Similarly the target elements are compressed, they experience resistance to radial expansion because of the surrounding constraining target material, and they also experience a shear resistance between the cylindrical element and the rest of the target as the cylinder is pushed forward. The resistance to radial extrusion due to surrounding confinement is in the form of an increment in flow stress as demonstrated in simple constrained compression tests [12, 16, 17], and the method is analogous to the approach taken in the analysis of indentation testing of semi-infinite metallic bodies [18]. The solution of the equations of motion for the element masses uses a finite difference technique [19, 20] to examine their motion as a function of time. Important to this study is that dynamic compression of material cylinders requires radial extrusion, and the associated radial acceleration of material is achieved at the expense of work done by the impacting projectile, and an associated increase in force for the compression of each cylindrical element. The force, F, for compression of a cylinder of diameter, d, and height, h, is given [15] by:

$$F = \frac{\pi}{4} d^2 Y \left[1 + \frac{3}{64} \rho \frac{V^2}{Y} \left(\frac{d}{h} \right)^2 \right] \tag{1}$$

where Y is the material flow stress, V is the velocity of compression (or the velocity difference across the element), and ρ is the material density.

In the right-hand side of Eqn (1), the first term is the resistance to compression due to material strength for simple uniaxial conditions, and the second term is the effect of radial acceleration of the material. The increased force is a direct outcome of the requirement to do work on ejecting material to increase its kinetic energy.

Erosion of penetrator (and target) material in the mushrooming model of Fig. 1(a) is achieved simply by removing elements as they reduce to less than one tenth of their original length, at which time the mass of the element in the line of penetration is considered to be contributing little to the total inertia of the stack of cylinders. This pragmatic approach avoided the difficulties of describing the shear removal of mass in a one-dimensional system.

A modified version of the original model is illustrated in Fig. 1(b) and is referred to as the erosion model. It uses the same element structure, consideration of compression, shear, confinement and radial inertia forces, and finite difference solution method as the mushrooming model. However, in it also considers that once material is extruded beyond the original diameter of the projectile it does not contribute to penetration of the target and is "eroded". Thus the effective hole diameter becomes the original projectile diameter, elements are of variable mass (i.e. they erode continuously as they are compressed and extruded), and the calculations of both the radial inertia term, Eqn (1), and the shear resistance to element movement are governed by the original projectile diameter, rather than an expanded element diameter as was the case with the mushrooming model with its constant mass elements. The structures of the models lead us to anticipate the mushrooming model. Fig. 1(a) will be a better approximation for low velocity impacts and underestimate depth of penetration, and the erosion model should be a better approximation for high velocity impacts and overestimate the depth of penetration.

The equations for solution in using the model are set out in difference form in the Appendix.

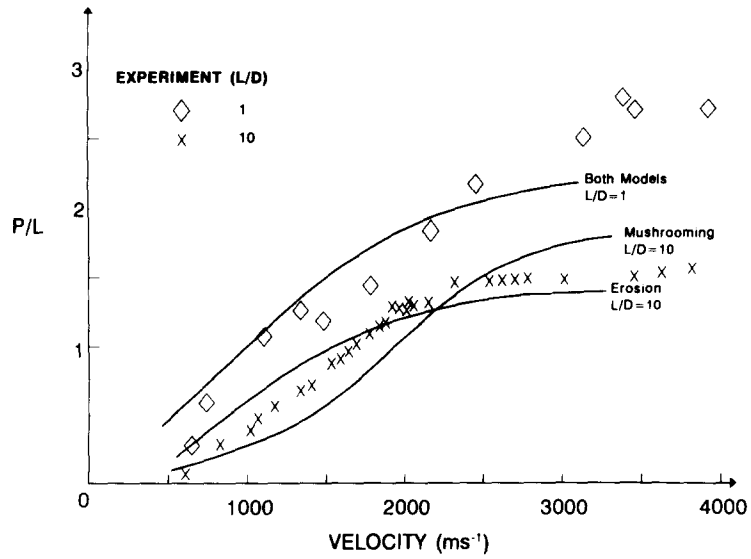

Fig. 2. Comparison of model predictions with experimental data for $L/D = 1$ and 10 tungsten alloy penetrators fired into steel targets. The model predicted results are shown by the continuous lines.

COMPUTATION RESULTS

The main features of model results are shown in calculations of depth of penetration compared with published experimental data [5–7] on tungsten alloy $L/D = 1$ and 10 penetrators fired into steel targets (Fig. 2). The mushrooming version tends to underestimate depth of penetration for high L/D penetrators, particularly when the velocity exceeds $1000\,\text{ms}^{-1}$, although at very high velocities, $>2500\,\text{ms}^{-1}$, it overestimates. The erosion version, on the other hand, overestimates depth of penetration for high L/D penetrators up to about $1700\,\text{ms}^{-1}$ but is a good match to experimental data above that velocity. For low L/D penetrators the two versions give similar results which are acceptably close to experiment. Clearly the model is capable of distinguishing the effect of L/D ratio, the main reason being the inclusion of the radial inertia term, Eqn (1), which is geometry dependent. For low L/D penetrators radial flow of material is difficult which is reflected in less penetrator deformation and smaller diameter, deeper penetration craters.

The effect of L/D ratio on penetrator performance is illustrated with a comparison between experimental data of Tate *et al.* [21] and calculations using the mushrooming version of the model in Fig. 3. The experimental data [21] included three groups of length to diameter ratio penetrator (L/D values 3, 6 and 12) and also three distinct penetrator masses in each group. The $L/D = 6$ data with its three distinct masses is compared with predictions of the mushrooming version of the model in Fig. 3(a) showing a different depth–velocity curve for each mass of penetrator (size indicated by diameter). When all nine sets of experimental data were consolidated and the parameter depth divided by penetrator diameter (P/D) plotted against velocity, then the nine distinct depth divided by velocity curves group into three bands each governed by the L/D ratio of the particular penetrators, as shown in Fig. 3(b). The mushrooming version of the model likewise condenses all the nine sets of computations into three corresponding P/D velocity curves. A similar grouping is found if depth divided by penetrator length (P/L) is plotted as in Fig. 3(c). Clearly the comparison of Fig. 3 shows that the mushrooming version of the model correctly calculates the effects of geometry on penetrator performance in both the magnitude and the phenomenological aspects. It is also clear from Fig. 3 that the quantitative agreement is better for low L/D ratio penetrators, and for the $L/D = 12$ penetrators this version of the model considerably underestimates depth of penetration above $1000\,\text{ms}^{-1}$ impact velocity.

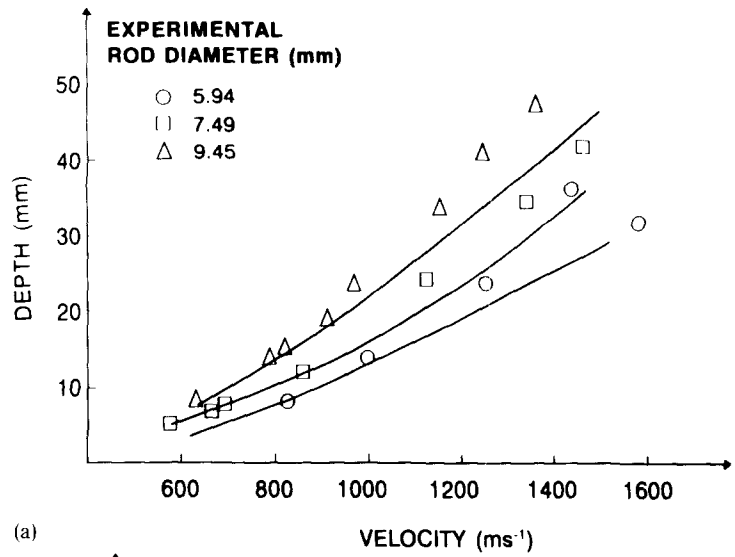

(a)

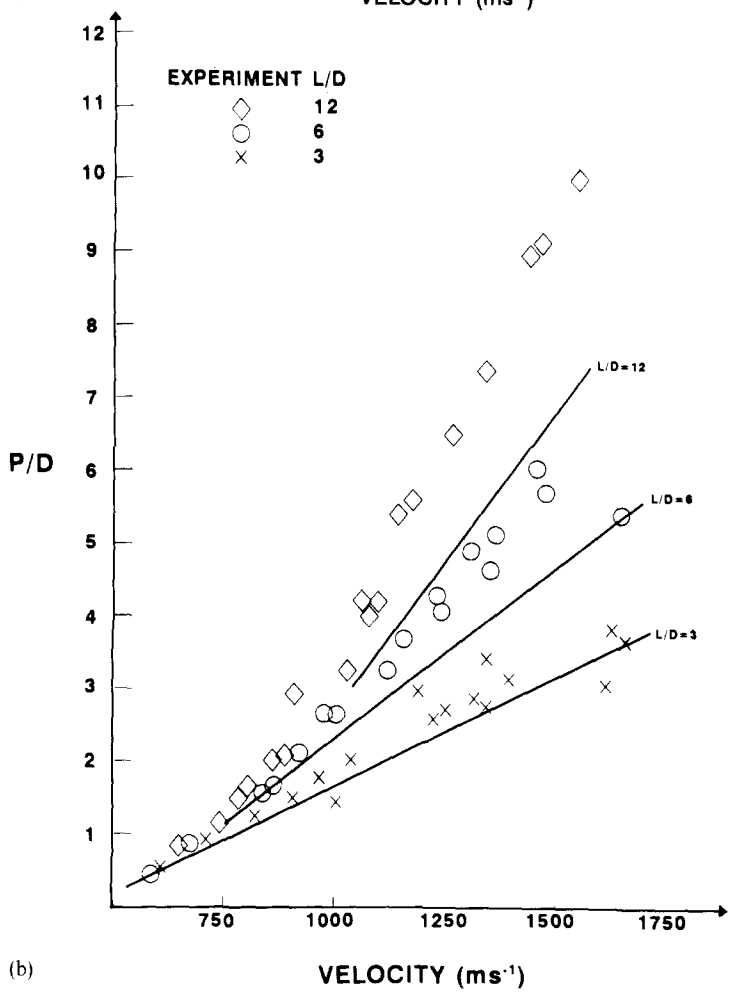

(b)

Fig. 3. Comparison of predictions of the mushrooming version of the model with experimental data of Tate *et al.* [21]: (a) depth as a function of velocity for $L/D = 6$ penetrators of three distinct masses (and corresponding rod diameter), (b) depth of penetration divided by projectile diameter (P/D) as a function of velocity for three L/D ratio and for each of the three projectile masses, and (c) depth of penetration divided by projectile intial length (P/L) as a function of velocity for the same nine data sets as in (b).

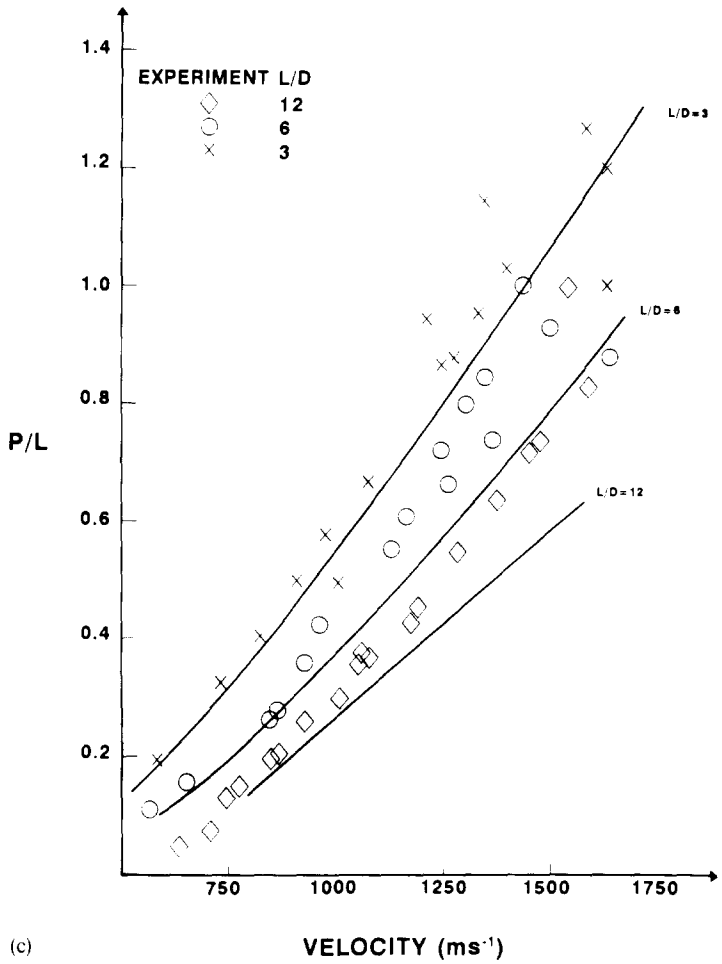

Fig. 3 (*Continued*)

A similar comparison to that above is shown in Fig. 4 for the erosion version of the model. Apart from the lowest L/D ratio case ($L/D = 3$), the erosion model overestimates depth of penetration. As Fig. 4(c) shows, the erosion model does not discriminate for different L/D ratios, as occurs in experiment at the lower velocities, however, above about $1600\,\mathrm{ms}^{-1}$ the model behaviour does mirror the experiment data.

Figure 5 shows a comparison of P/L vs velocity data for a range of experiments as presented by Rosenberg and Dekel [9] for L/D 10, 20 and 23 penetrators and for both versions of the model. The mushrooming version comparison, Fig. 5(a), shows an underestimate of depth of penetration but a clear separation of results on the basis of L/D ratio. The erosion version, Fig. 5(b), gives a better estimate of the magnitude of the depth of penetration and again discriminates on the basis of L/D ratio with the magnitude of the L/D effect being similar to that shown in the experimental results. As with the earlier cases the erosion version of the model overestimates depth of penetration at low velocities, but tends to predict correctly from about $1600\,\mathrm{ms}^{-1}$ impact velocity and higher.

In Fig. 6 is shown experimental data of Magness and Leonard [10] for the penetration of $L/D = 19$, full-scale, DU penetrators and for $L/D = 20$, full-scale, tungsten, as well as one quarterscale tungsten and DU penetrators, compared with calculations using the erosion version of model. The ordering of experimental data with DU performing better than tungsten alloy and with full-scale penetrators performing better than quarterscale penetrators is reflected in the computational predictions. As in the previous examples, the mushrooming model underestimated depth of penetration substantially for these penetrators and at this velocity range. Although the correct ordering of data is reflected by the erosion

version, the uncertainty in the calculations is only of the order of the width of the interval between the lower three sets of computational results. This uncertainty in the calculations results from the size of the time step, element size and minimum thickness when an element is considered as no longer to contribute to penetration capability (one-tenth original height). The difference between tungsten and DU in the model computations results from differences

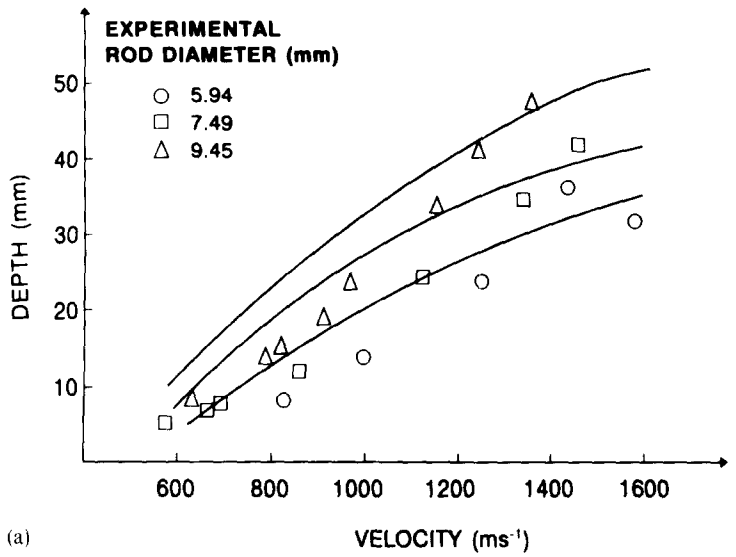

(a)

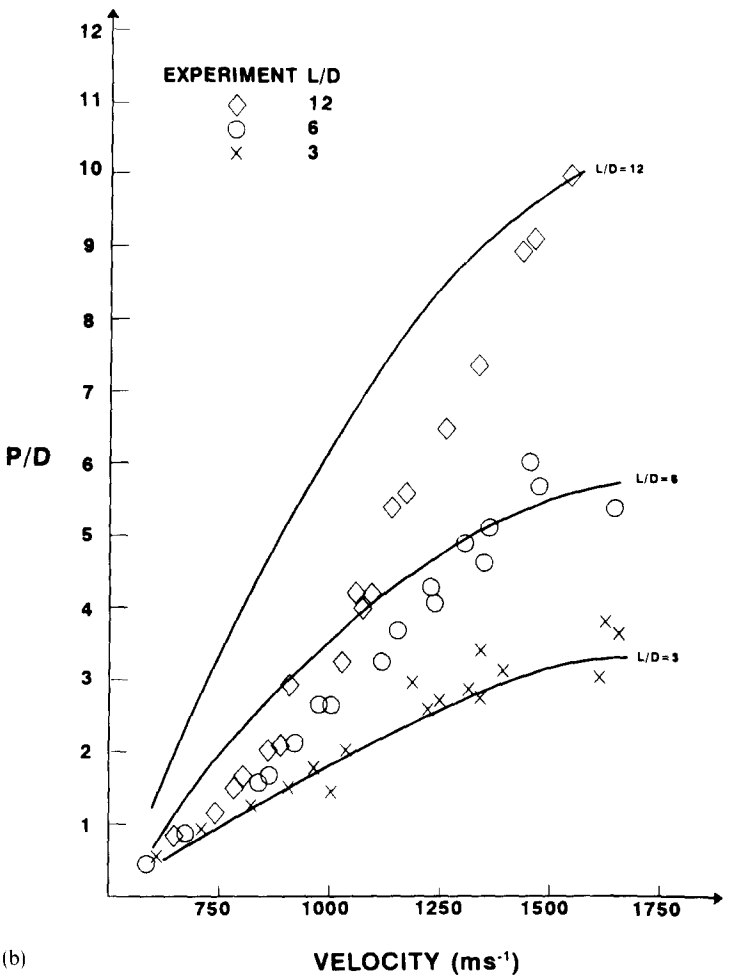

(b)

Fig. 4. Comaprison of predictions of the erosion version of the model with the experimental data of Tate *et al.* [21] with (a), (b) and (c) being depth, P/D and L/D respectively as in Fig. 3.

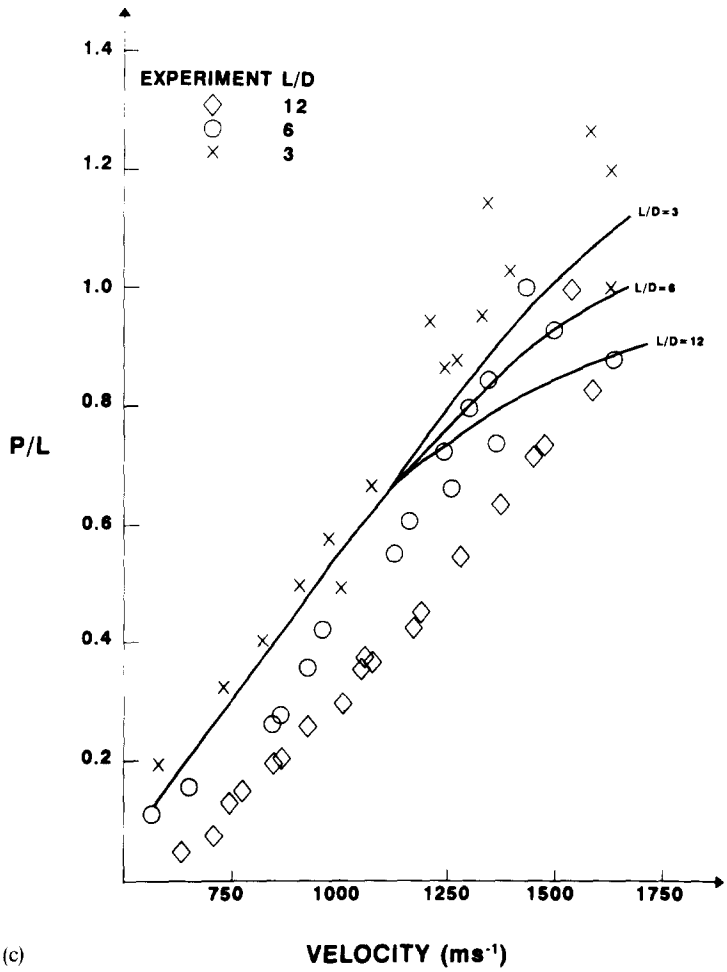

(c)

Fig. 4 (*Continued*)

in properties used for the calculation, the principal ones being σ_0 and n in the constitutive relation adopted:

$$\sigma = \sigma_0 \varepsilon^n \tag{2}$$

where σ is stress and ε is strain. Values used for σ_0 and n were 2440 MPa and 0.118 respectively for DU and 1967 MPa and 0.25 for the tungsten alloy. The model does not include aspects related to the physics of failure which are normally linked with the difference in performance between tungsten alloy and DU penetrators. The debate is still open on what causes deeper penetration for DU compared to tungsten alloy penetrators because Kimsey and Zook *et al.* [22] have shown that the inclusion of thermal softening into code simulations of tungsten alloy penetrators allows deeper penetration, of the order of magnitude expected from the difference between DU and tungsten alloy performances and without adiabatic shear failure considerations. This accords with the differences based on strength shown in Fig. 6, although the present model is not written to include thermal softening explicitly at this stage. Although at the scale difference of Fig. 6 (full-scale and one-quarter) it is possible to distinguish scale effects, this was not possible in the data of Figs 3(a) and 4(a) when that data is regrouped as P/L in Figs 3(c) and 4(c) respectively, because in these cases differences in scale are getting very small.

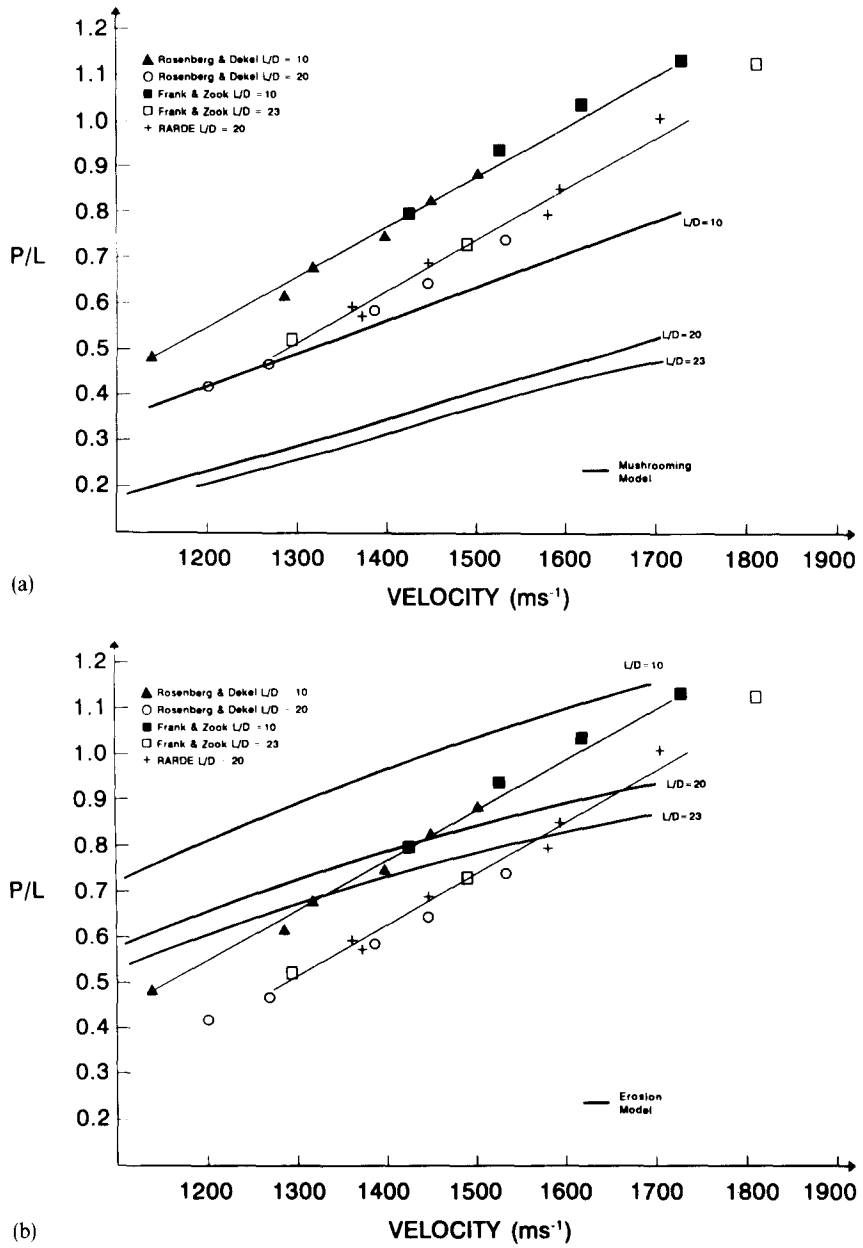

Fig. 5. Comparison of experimental data presented by Rosenberg and Dekel [9] with predictions using the two versions of the model as shown by the heavier lines with L/D values indicated: (a) the mushrooming version and (b) the erosion version of the model.

DISCUSSION

It should be understood that we are carrying out computations on model problems. To the extent that the processes represented in the model problem describe in a correct mathematical form physical phenomena in the real world, and if there is a reasonable concurrence of computational results with experimental data, then the model is useful. The present computations demonstrate that the inclusion of terms accounting for both radial inertia effects and shear allow correct modelling of the effect of penetrator L/D ratio on depth of penetration. The approach used also shows differences on the basis of scale and material which mirror experimental data. It is suggested that including these aspects of the physics of penetration into the modified hydrodynamic approach may allow that model to also

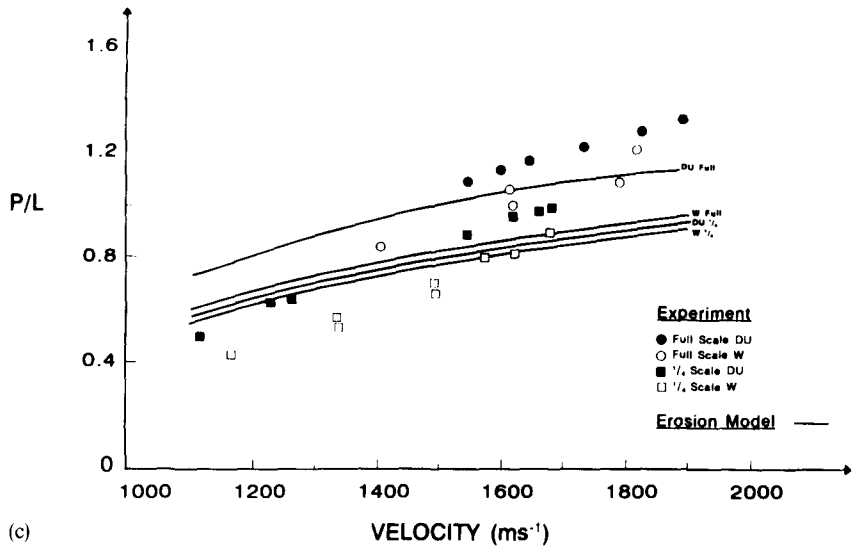

Fig. 6. Comparison of computations using the erosion version of the model with experimental data of depleted uranium (DU) and tungsten (W) alloy penetrators at both full scale and one quarter scale.

distinguish effects due to L/D ratio, scale and material. Because the influences of friction and radial inertia only occur at the projectile tip where deformation is occurring, and because of their dependence on the geometry of the deforming region, it may be required that the modified hydrodynamic model be formulated with the penetrator and target being segmented into elements as is done in the present approach.

Both versions of the model bear similarities to the concepts put forward by Recht [23] which see penetration by deforming projectiles as a balance between projectile mushrooming and shear of displaced material, features which are clearly evident in sectioned penetrators [24]. The mushrooming version of the present model as originally formulated, Fig. 1(a), assumes that the whole rod is carried forward, with shear in the penetrator and target occurring at the diameter of the interface element which can reach up to 3.2 times the original diameter before the element is removed as being ineffective. Whilst this appears to be reasonable for the prediction of depth of penetration at low velocities, where erosion is not generally observed in experimental impacts, it leads to an underestimate of depth of penetration, for high L/D penetrators in particular, at high velocities above about $1000\,\mathrm{ms}^{-1}$. The assumption of continuous erosion so that the target is loaded and perforated at the diameter of the original penetrator, as in Fig. 1(b), leads to an overestimate of the depth of penetration at velocities up to about $1500\,\mathrm{ms}^{-1}$ for high L/D ratio penetrators. Clearly both models embody aspects that are realistic, but the appropriate model is somewhere between these extremes.

A close examination of the comparisons of Figs 2–6 shows some disagreements between the model computations and experiment in addition to the differences in magnitude mentioned above. Most noticeable in Figs 5 and 6 are the slopes of the P/L vs velocity relations. The extent to which these differences are due to the approximations in one-dimensional modelling, or to approximate computational procedures, is uncertain. For the simpler problem of projectile mushrooming against a rigid wall, it has been demonstrated that in using a model which is segmented into elements, shear between elements as well as element compression is important, and the inclusion of a term to account for this would be expected to improve the present solution [25, 26]. The present solution methods would also be improved by using a variable time step which would allow a smaller minimum element height, by giving attention to the effect of element height, and also to the physics of erosion (if this is possible in a one-dimensional approach). The extent to which the material differences demonstrated in Fig. 6 are due to fortune or are a real reflection of the physics of penetration

is uncertain because the material model used is very approximate, particularly as far as failure and erosion are concerned. Nevertheless it reflects recent indications that material differences based on flow stress may explain the DU-tungsten alloy performance gap. The inclusion of thermal softening in the present model should be possible and would be expected to improve the concordance between model predictions and experiment. Differences between the model and experiment are not generally attributable to rate effects, because when this is simulated by modifying the constitutive parameters appropriately, the fit to experimental data is not radically improved.

CONCLUSIONS

Modelling of penetration using a one-dimensional model is used to demonstrate that including the effects of radial inertia and shear between the penetrator and the target allows correct modelling of L/D effects, as well as the effects of penetrator scale and material. The two versions of the model used which assume penetrator mushrooming behaviour and penetrator erosion respectively, bound penetrator performance at high velocities and high L/D ratios. Both models give reasonable predictions of penetrator behaviour for low L/D ratio penetrators.

REFERENCES

1. T. W. Wright, A survey of penetration mechanics for long rods. In *Computational Aspects of Penetration Mechanics*, pp 85–106. (Edited by J. Chandra and J. E. Flaherty.) Springer-Verlag, Berlin (1983).
2. V. P. Alekseevkii, Penetration of a rod into a target at high velocity. *Fiz. Goren. Vzryra* **2**, 99 (1966).
3. A. Tate, A theory for the deceleration of long rods after impact. *J. Mech. Phys. Solids* **15**, 387–399 (1967).
4. A. Tate, Further results in the theory of long rod penetration. *J. Mech. Phys. Solids* **17**, 141–150 (1969).
5. V. Hohler and A. J. Stilp, Hypervelocity impact of rod projectiles with L/D from 1 to 32. *Int. J. Impact Engng* **5**, 323–331 (1987).
6. G. Weihrauch and E. Wollmann, Segmented penetrators. *Propellants, Explosives, Pyrotechnics* **18**, 270–274 (1993).
7. A. C. Charters, T. L. Menna and A. J. Piekutowski, High velocity penetration of semi-infinite steel by continuous and segmented rods. In *Shock Compression of Condensed Matter—1989*, pp. 931–934 (Edited by S. C. Schmidt, J. N. Johnson and L. W. Davison.) Elsevier Science (1990).
8. K. Frank and J. Zook, Chunky metal penetrators act like constant mass penetrators. *Proc. 12th Int. Symp. on Ballistics*, Vol. 1, pp. 441–449, ADPA, San-Antonio, Texas, Oct. (1990).
9. Z. Rosenberg and E. Dekel, The relation between the penetration capability of long rods and their length to diameter ratio. *Int. J. Impact Engng* **15**, 125–129 (1994).
10. L. Magness Jr and W. Leonard, Scaling issues for kinetic energy penetrators, *Proc. 14th Int. Symp. on Ballistics*, pp. 281–289 ADPA, Quebec, Canada, Sept. (1993).
11. Z. Rosenberg and E. Dekel, A critical examination of the modified Bernoulli equation using two-dimensional simulations of long rod penetrators. *Int. J. Impact Engng* **15**, 711–720 (1994).
12. R. L. Woodward, Penetration of semi-infinite metal targets by deforming projectiles. *Int. J. Mech. Sci.* **24**, 73–87 (1982).
13. R. L. Woodward, Appraisal of a one-dimensional ballistic penetration model. *Proc. 7th Int. Symp. on Ballistics*, pp. 281–287, ADPA, The Hague, Netherlands, April (1983).
14. C. E. N. Sturgess and M. G. Jones, Estimation of dynamic forces in high speed compression using a free flight impact forging device. *Int. J. Mech. Sci.* **13**, 309–322 (1971).
15. W. Johnson. *Impact Strength of Materials*, p. 152. Arnold (1972).
16. R. L. Woodward and M. E. deMorton, Penetration of targets by flat-ended projectiles. *Int. J. Mech. Sci.* **18**, 119–127 (1976).
17. J. Liss, W. Goldsmith and F. E. Hauser, Constraint to side flow in plates. *Trans. ASME, J. Appl. Mech.* **50**, 694–698 (1983).
18. D. Tabor, The hardness and strength of metals. *J. Inst. Met.* **79**, 1–18 (1951).
19. M. S. J. Hashmi and P. J. Thompson, A numerical method of analysis for the mushrooming of flat-ended projectiles impinging on a rigid anvil. *Int. J. Mech. Sci.* **19**, 273–283 (1977).
20. R. L. Woodward and J. P. Lambert, A discussion of the calculation of forces in the one-dimensional finite difference model of Hashmi and Thompson. *Int. J. Mech. Sci.* **23**, 497–501 (1981).
21. A. Tate, K. E. B. Green, P. G. Chamberlain and R. G. Baker, *Proc. 4th Int. Symp. on Ballistics*, ADPA, Monterey, California, Oct. (1978).
22. K. D. Kimsey, L. S. Magness, J. A. Zook and K. Frank, work discussed in L. S. Magness, D. Kapoor and R. Dowding, Novel flow-softening and flow anisotropy approaches to developing improved tungsten kinetic energy penetrator materials. *U.S. Army Science Conf.* (1994).
23. R. F. Recht, Taylor ballistic impact modelling applied to deformation and mass loss determinations. *Int. J. Engng Sci.* **16**, 809–827 (1978).
24. R. L. Woodward, Material failure at high strain rates. In *High Velocity Impact Dynamics*, pp. 65–125 (Edited by J. A. Zukas.) J. Wiley, N.Y. (1990).

25. R. L. Woodward, B. J. Baxter and N. M. Burman, The use of blunt projectile impact for the characterisation of dynamic material constitutive behaviour, *Proc. 14th Int. Symp. on Ballistics*, pp. 321–330, ADPA, Quebec, Canada, Sept. (1993).
26. R. L. Woodward, N. M. Burman and B. J. Baxter, An experimental and analytical study of the Taylor impact test. *Int. J. Impact. Engng* **15**, 407–416 (1994).

APPENDIX: SOLUTION METHOD

The equations and solution method are set out below consistent with the notation used in earlier work [12] which described the mushrooming version of the model, and showing the modifications to the equations for the erosion version of the model.

Referring to Fig. 1, the equtions of motion are:

$$N_{i+1,j} - N_{i,j} - T_{i,j} - m_{i,j}\ddot{u}_{i,j} = 0 \tag{A1a}$$

$$N_{i,j} - N_{i-1,j} + T_{i,j} - m_{i,j}\ddot{u}_{i,j} = 0 \tag{A1b}$$

where $N_{i,j}$ is the normal force on element i at time step j

$T_{i,j}$ is the shear force

$\ddot{u}_{i,j}$ is the acceleration

and $m_{i,j}$ is the element mass.

Equation (A1a) applies to the cylinder representing the projectile and Eqn (A1b) to the cylinder representing the target. Elements, i, are numbered starting from the non-impact end of the projectile. The element mass is constant for the mushrooming version of the model until it is deleted when its height is reduced by compression to one tenth the original value and it is considered no longer to be contributing to the problem, but continuously variable for the erosion version of the model. Thus

$$m_{i,j} = m_{i,0} \tag{A2a}$$

$$m_{i,j} = m_{i,0}h_{i,j}/h_{i,0} \tag{A2b}$$

where $h_{i,j}$ is the element height,
apply to the mushrooming version of the model, Eqn (A2a), and to the erosion version of the model, Eqn (A2b), respectively. The zero subscript specifies the value of the element mass at the time of impact.

The relationship between acceleration, $\ddot{u}$, and displacement, u, is

$$u_{i,j+1} = \ddot{u}_{i,j}(\delta t)^2 + 2u_{i,j} - u_{i,j-1} \tag{A3}$$

where the time increment, δt, is given by

$$\delta t = t_{j+i} - t_j. \tag{A4}$$

Plastic deformation is treated using a constitutive equation of the form

$$\sigma = \sigma_0 \varepsilon^n \tag{A5}$$

where σ is normal stress

ε is normal strain calculated as the natural logarithm of the current over the initial element height

and constants σ_0 and n are material specific and obtained from simple compression tests. Elastic unloading and re-loading to yield uses the relation

$$\sigma = \varepsilon \mathrm{E} + C \tag{A6}$$

where E is the material Young's modulus and the constant C is calculated at each step based on the last point of strain at plastic yield.

To account for confinement the target flow stress is incremented by a factor 2.7, and with $_\mathrm{T}$ denoting target and $_\mathrm{p}$ denoting projectile, the actual normal stress to deform a target element is

$$\sigma_\mathrm{T} = 2.7\sigma_{0\mathrm{T}}\varepsilon^{n_\mathrm{T}} \tag{A7a}$$

and for the projectile

$$\sigma_\mathrm{p} = \sigma_{0\mathrm{p}}\varepsilon^{n_\mathrm{p}} \tag{A7b}$$

or

$$\sigma_\mathrm{p} = \sigma_{0\mathrm{p}}\varepsilon^{n_\mathrm{p}} + 1.7\sigma_{0\mathrm{T}} \tag{A7c}$$

where Eqn (A7b) applies for elements of the projectile which are not inside the target or which have a diameter less than the interface element diameter, and Eqn (A7c) applies for elements which are both inside the target and whose diameter also equals or exceeds the projectile interface element diameter. For the erosion model, as distinct from the mushrooming version, confinement, Eqn (A7c), is allowed for all projectile elements within the target which have deformed, and for all other projectile elements Eqn (A7b) is used. The inclusion of the increment due to target strength in Eqn (A7c) and the assumption of projectile interface element diameter defining the instantaneous target hole diameter, have been discussed at length elsewhere [12]. The depth of penetration is taken from the original target element interface position, and the target is made sufficiently thick that movement of the last element is negligible up to the time penetration ceases.

The increment in stress due to radial inertia, σ_r is calculated from the equations

$$\sigma_{ri} = \frac{3}{64}\rho_p\left(\frac{D_i}{h_i}\right)^2 (\dot{u}_j - \dot{u}_{i-1})^2 \tag{A8a}$$

$$\sigma_{ri} = \frac{3}{64}\rho_T\left(\frac{D_i}{h_i}\right)^2 (\dot{u}_{i-1} - \dot{u}_i)^2 \tag{A8b}$$

where D_i is element diameter

$\dot{u}_i$ is element velocity

and $\rho_p$and ρ_T are material density for projectile and target respectively.

Equation (A8a) refers to the projectile and Eqn (A8b) to the target. For the erosion version of the model, D_i becomes $D_{i,0}$, or the original element diameter, in Eqn (A8) because any material beyond this is eroded continuously.

The shear force at the side of the element, T, is calculated from

$$|T_{i,j}| = \frac{\pi}{\sqrt{3}} D_{i,j} h_{i,j} \sigma_0^* \tag{A9a}$$

$$|T_{i,j}| = \frac{\pi}{\sqrt{3}} D_{pi,j} h_{,j} \sigma_{0T} \tag{A9b}$$

where $D_{i,j}$ is the element diameter

$D_{pi,j}$ is the projectile interface element diameter.

Equation (A9a) applies to a projectile element, under the same restrictions as confinement is included as per Eqn (A7c), and Eqn (A9b) applies to target elements. The sign of the shear force is governed by the direction of movement and σ_0^* is the lesser of σ_{0p} and σ_{0T}. Equation (A9) apply for the mushrooming version of the model as they are, however for the erosion version the diameter terms become the intitial projectile diameter and σ_0^* is always taken as equal to σ_{op}.

The normal force on an element is the sum of a confined or an unconfined strength term, Eqn (A7), and the radial inertia term, Eqn. (A8). Thus

$$N_{i,j} = [\sigma_{i,j}(\varepsilon) + \sigma_{ri,j}]A_{i,j} \tag{A10}$$

where the material stress $\sigma_{i,j}$ is a function of strain, ε, and $A_{i,j}$ is the element diameter, calculated by assuming constant volume deformation for the mushrooming version of the model, and using the initial projectile cross section area for the erosion version of the model.

The problem is initiated with projectile elements moving with the initial velocity, v_0, and target elements stationary, except that the masses of the projectile and target interface elements are combined, as in Fig. 1, and given a velocity v, calculated by

$$\tfrac{1}{2}(m_{op} + m_{oT})v^2 = \tfrac{1}{2}m_{op}v_0^2 \tag{A11}$$

where the zero subscript again refers to the initial value. Initially forces are all zero so in the first time step Eqns (A1 and A3) can be used to calculate displacements, element strains, and velocities, and new element positions are logged. Then new stress and force values can be calculated with Eqns (A7–A10). These values are substituted into (A1) and the cycle repeated. The forces at the ends of the projectile and target away from impact remain zero throughout. If an element is eroded a form of Eqn (A11) defines the new interface velocity. The calculations involve repetitions of this cycle and the remainder of the computer program is concerned with updating and logging parameters. The calculation is stopped when the projectile velocity drops below a specified level (say 10 ms^{-1} for a practical ballistic impact), or when the projectile is completely eroded.